International Journal of Biological Macromolecules 195 (2022) 589–597

Contents lists available at ScienceDirect

International Journal of Biological Macromolecules

journal homepage: www.elsevier.com/locate/ijbiomac

Molecular imprinting based electrochemical biosensor for identification of serum amyloid A (SAA), a neonatal sepsis biomarker

Sapna Balayan [a], Nidhi Chauhan [a], Ramesh Chandra [b,*], Utkarsh Jain [a,*]

[a] Amity Institute of Nanotechnology (AINT), Amity University Uttar Pradesh (AUUP), Sector -125, Noida-201313, Uttar Pradesh, India
[b] Drug Discovery and Development Laboratory, Department of Chemistry, University of Delhi, Delhi -110007, India

ARTICLE INFO

Keywords:
Biomarker
Polymer
Serum amyloid A
Biosensor
Electrochemical
Sepsis

ABSTRACT

Neonatal septicemia is a bacterial infection in newborns. It is caused by bacteria including *Escherichia coli* and Group B *Streptococcus (*GBS). Neonatal septicemia is divided into early-onset and late-onset sepsis. The diagnosis of neonatal septicemia is a challenging task because of the presence of nonspecific symptoms. Biomarkers such as C-reactive protein (CRP), procalcitonin (PCT), and serum amyloid A (SAA) can help in the detection of sepsis at early stages. The level of biomarkers is elevated once sepsis occurs in the body. This study presents the development of an electrochemical biosensor based on nanomaterials integrated molecularly imprinted polymer technique. To obtain the synergistic effect and high conductivity, multi-walled carbon nanotubes (MWCNTs), manganese oxide nanospheres (MnO_2NSs), and cobalt oxide nanoparticles (Co_3O_4NPs) were coated over the screen-printed electrode (SPE). A further modification was done by polymerizing molecularly imprinted polymer (MIP) specifically synthesized for SAA onto modified SPE. The performance of the designed platform was evaluated through electrochemical techniques. The operating range of the developed sensor was found to be 0.01 pM to 1 μM and 0.01 pM as the lower detection limit.

1. Introduction

Neonatal septicemia (NS) is a bloodstream infection. It is the leading cause of high mortality and morbidity in newborns worldwide. Approximately 3 to 40 per 1000 lives are affected by NS condition and the mortality rate of affected newborns varies from 9% to 20% [1]. The reported data indicates that approximately 30–50% of neonates deaths occur each year as a result of NS [2,3]. NS is considered as a clinical syndrome that occurs in the first 90 days of life. It is caused by bacteria in bloodstreams such as Group B *Streptococcus* (GBS), *Klebsiella* spp., non-typhoid *Salmonella*, and *Escherichia coli* (*E. coli)* [2,4,5]. Depending upon the time of onset, NS is classified into two categories: early-onset sepsis (EOS) and late-onset sepsis (LOS). The symptoms and signs of sepsis are not specific, which poses challenges in its early detection. The treatment is delayed due to their non-specific symptoms of septicemia causing serious problems including organ failure and death. Septicemia can be diagnosed with microbial analysis and biomarker screening. The microbial analysis method requires 2–5 days to analyze blood samples from neonates. Whereas, if the pathogens are very sensitive, slow-growing, or if antibiotic treatment is provided, the sensitivity of the test is reduced. In certain cases, septicemia could not be diagnosed by microbial tests. Therefore, it is recommended to perform a biomolecule screening test (such as C-reactive protein (CRP), complete blood count (CBC), procalcitonin (PCT), differential leukocyte counts, serum amyloid A (SAA), and neutrophil counts) [2,3,6]. The detection of these biomarkers can also be obtained with an enzyme-linked immunosorbent

Abbreviations: NS, neonatal septicemia; GBS, Group B *Streptococcus*; EOS, early-onset sepsis; SAA, serum amyloid A; ELISA, enzyme-linked immunosorbent assay; MWCNTs, multi-wall carbon nanotubes; MnO_2NSs, manganese dioxide nanospheres; Co_3O_4NPs, cobalt oxide nanoparticles; NPs, nanoparticles; LOS, late-onset sepsis; MIP, molecularly imprinted polymer; *E. coli*, *Escherichia coli*; $MnSO_4.H_2O$, manganese sulfate monohydrate; H_2SO_4, sulfuric acid; SEM, scanning electron microscopy; CBC, complete blood count; $Co(CH_3COO)_2{\cdot}4H_2O$, cobalt(II) acetate tetrahydrate; CRP, C-reactive protein; AIBN, azobisisobutyronitrile; MMA, Methyl methacrylate; EGDMA, ethylene glycol dimethacrylate; ACN, acetonitrile; $KMnO_4$, potassium permanganate; SRL, Sisco Research Laboratories Pvt. Ltd; SPE, screen-printed electrode; DW, distilled water; XRD, X-Ray diffraction; PCT, procalcitonin; CV, cyclic voltammetry; NIP, non-imprinted polymer; MIP_{SAA}, molecularly imprinted polymer with template; EIS, electrochemical impedance spectroscopy; Rct, resistance charge transfer; DPV, differential pulse voltammetry; $C_6H_8O_6$, ascorbic acid; $C_{27}H_{46}O$, cholesterol; $C_6H_{12}O_6$, glucose; $C_5H_4N_4O_3$, uric acid; Ach, acetylcholine.

* Corresponding authors.
E-mail addresses: acbrdu@hotmail.com (R. Chandra), ujain@amity.edu (U. Jain).

https://doi.org/10.1016/j.ijbiomac.2021.12.045
Received 13 May 2021; Received in revised form 6 October 2021; Accepted 6 December 2021
Available online 14 December 2021

assay (ELISA). This method also has certain limitations like time consumption, requires trained users, producing false-negative and positive results, require large sample volume, antibody instability, and is expensive [11–14]. These limitations can be overcome by developing an electrochemical biosensor.

SAA is an acute-phase reagent like CRP and PCT. SAA levels have been reported to change during inflammation [7]. It consists of a polymorphic apo-lipoprotein having a molecular weight of approximately 12 kDa. The synthesis of SAA in the body is carried out in the liver. The available data show that during infection increase in the level of SAA is occurred indicating SAA is an acute phase reactant for the detection. The analysis of SAA level also helps to detect cardiac, viral, and traumatic conditions. The level of SAA is dependent upon the age factor. The minimum concentration of SAA is recorded in umbilical cord blood, whereas higher concentrations of SAA are found in grown-up persons. Because of the dynamic elevation in the level of SAA during inflammation, it can play a leading role in the diagnosis of EOS comparing to the CRP. The level of SAA is firstly increased in the body of infected newborns and subsequently decreases [8–10].

In this study, an electrochemical biosensing platform was fabricated for determining SAA concentration in blood samples from newborns. The electrode was embedded with nanomaterials multi-wall carbon nanotubes (MWCNTs), manganese dioxide nanospheres (MnO_2NSs), cobalt oxide nanoparticles (Co_3O_4NPs) to improve the significant parameters including conductivity, rapid results, sensitivity, specificity, and repeatability of the developed biosensor. The surface of the screen-printed electrode was altered with MWCNTs. MWCNTs show dual properties such as providing higher electronic conductivity and immense support for the biological compounds. In addition, once integrated with MnO_2NSs, a higher surface-to-volume ratio is achieved. MnO_2NSs exhibit excellent chemical and physical properties such as good permeability, higher energy density, and catalytic ability [15–18]. Furthermore, the electrode was modified using Co_3O_4NPs. The Co_3O_4NPs have wide applications in energy storage systems [19], electrochromic and heterogeneous catalysts resulting in an improved optical, electrocatalytic, magnetic, and semiconducting properties. Additionally, they exhibit large surface area, excellent conductivity, and reversibility during the charging and discharging process. These NPs contribute to the fast and easy transfer of electrons resulting in good reversibility of the system [20–23]. The synergic effect of Co_3O_4NPs/MnO_2NSs/MWCNTs can facilitate the large surface area on the electrode, higher conductivity, and catalytic properties of the developed biosensor.

Molecular imprinting is a template-based technique, where specific recognition sites can be developed for biomolecules such as proteins, antibodies, amino acids, and enzymes [24]. For preparing molecularly imprinted polymer (MIP), a composition of template, monomer, and crosslinker is prepared in the porogen solvent. Thereafter, the specific cavities for the template are created by the polymerization of the monomer around a template. Further, the template molecule is removed from this polymer structure and binding sites complementary to the template (orientation, structure, and size) are obtained. The specific cavities obtained after the removal of the template serve as a functional recognition site for SAA binding [25].

The MIPs have high sensitivity, selectivity, stability and require low cost for the synthesis process [26,27]. These properties of MIP enable their use in the development of an electrochemical biosensing platform in diverse fields such as environmental science, pharmaceutical, forensic, and life sciences [28–31]. Only limited studies have been reported for the development of an electrochemical biosensor for SAA. Therefore, developing a MIP-based sensing platform can advance in the early, rapid, and significant detection of SAA levels during inflammation [25].

2. Experimental measurements

2.1. Chemicals and apparatus

Multi-walled carbon nanotubes, manganese sulfate monohydrate ($MnSO_4.H_2O$), sulfuric acid (H_2SO_4), ethylene glycol dimethacrylate (EGDMA), cobalt(II) acetate tetrahydrate ($Co(CH_3COO)_2{\cdot}4H_2O$), ammonia solution, methanol, acetic acid, azobisisobutyronitrile (AIBN, 98%), methyl methacrylate (MMA), potassium permanganate ($KMnO_4$), acetonitrile (ACN), were purchased from Sisco Research Laboratories Pvt. Ltd. (SRL), India. Serum amyloid A was obtained from the US-based company Sigma-Aldrich. The biosensor was developed on the surface of a screen-printed electrode (SPE) (dimension 8 × 10 and geometric area 7.07 mm^2). These electrodes were acquired from a Netherland-based company PalmSens Compact Electrochemical Interfaces. Distilled water (DW) was used in the preparation of the solution during the experiments.

The modified surface of the electrode was determined with scanning electron microscopy (SEM), and X-Ray diffraction (XRD). The electrochemical studies were then carried out using Biologics potentiostat (specification: SP-150, EC-Lab software). The electrochemical cell is a system composed of three electrodes (working, referential and auxiliary). The flow of electrons in the electrochemical system takes place in the presence of an electron mediator.

2.2. Synthesis of MnO_2 hollow nanospheres

The synthesis of hollow MnO_2NSs was performed as reported earlier [32]. A mixture of $MnSO_4.H_2O$ (8.50 g) and $KMnO_4$ (3.43 g) powder was prepared, and grind into fine particles in a ratio of 4:3 M concentrations at room temperature. Subsequently, the prepared mixture was dissolved in 200 mL of DW with continuous stirring. For removing potassium anions and catalyzing the experiment, 100 mL of H_2SO_4 solution was added to the mixture with vigorous stirring (30 min.). To accelerate the crystallization process, the solution was placed in a water bath at 60°C for 30 min. The product was filtered and washed by using DW (3 times). The last washing was performed with ethanol to remove unbound reagents. The black color product was obtained and then dried overnight at 70°C in a vacuum oven [32]. The following equation describes a chemical reaction for the synthesis of MnO_2NSs.

$$3Mn^{2+}\ (aq.) + 2MnO_4^-\ (aq) + 2H_2O\ (L) \rightarrow 5MnO_2\ (s) + 4H^+\ (aq.)$$

2.3. Preparation of cobalt oxide nanoparticles

The preparation of Co_3O_4NPs was carried out by the decomposition method [33]. A solution was prepared in 25 mL of DW containing 0.50 g of $Co(CH_3COO)_2{\cdot}4H_2O$ (0.50 g), then 25 mL of ammonia (25%) was dropwise added under vigorous stirring into the mixture. The mixture was kept for stirring for 10 min. (at room temperature) to form a homogeneous fuscous slurry. The prepared mixture was autoclaved at 150 °C for 3 h. The resulting black solid product was washed with DW 3 times and dried at 60 °C for 4 h [33].

2.4. Synthesis of molecularly imprinted polymer for SAA

The MIP for SAA was synthesized using a precipitation polymerization process. The SAA (template), EGDMA (crosslinker), MMA (monomer) were added to a specific ratio (1:4:4) in a 20 mL of porogen (ACN). Then, the mixture was sonicated for 45 min at room temperature, and treated with nitrogen gas for 10 min. A 100 mg AIBN (initiator) was added to the mixture to initiate the polymerization process. The mixture was sealed under inert conditions and kept for polymerization at 35°C for 48 h in a water bath. The synthesized polymer was washed with a solution of methanol and acetic acid (ratio 4:1) for 24 h. The final washing of the product was carried out with methanol to remove chemical

residues. The obtained polymer was dried and crushed into a fine powder (Scheme 1).

2.5. Assembling of working SPE

2.5.1. Electrodeposition of MWCNTs on SPE

A solution of 10 mg MWCNTs was prepared in a 1 mL mixture of H_2SO_4 and HNO_3 (ratio 3:1). The solution was then sonicated for 30 min. Thereafter, a 100 μL solution was used for electrodeposition by cyclic voltammetry (CV) on the surface of the working electrode. The potential was applied from −1.0 to +1.0 V for 20 CV cycles (scan rate 50 mV/s) in a mediator solution of 0.5 mM (Ferri-Ferro) [34].

2.5.2. Modification of MWCNTs/SPE electrode with MnO_2NSs

A suspension was prepared with 10 mg of MnO_2NSs in 1 mL DW. The mixture was sonicated for 1 h. A 100 μL of this prepared solution was used for electrodeposition of MnO_2NSs on the surface of MWCNTs/SPE. Cyclic voltammetry was used for modifying the electrode with applied potential ranging from −0.2 to +0.6 V for 20 CV cycles (50 mV/s scan rate) in the Ferri-Ferro mediator solution [15]. The modified electrode was dried at room temperature and used for further experimentations.

2.5.3. Deposition of Co_3O_4NPs on MnO_2NSs/MWCNTs/SPE

A solution was prepared in 1 mL DW with 10 mg Co_3O_4NPs and kept on sonication for 1 h. The Co_3O_4NPs were deposited on modified MnO_2NSs/MWCNTs/SPE electrode through the process of CV with potential ranging from −0.2 to +0.7 V (scan rate 50 mV/s) for 10 cycles in a Ferri-Ferro mediator solution.

2.5.4. Integration of MIP on modified Co_3O_4NPs/MnO_2NSs/MWCNTs/SPE electrode

Further, the electrode was moderated with MIP deposition, on the surface of the modified Co_3O_4NPs/MnO_2NSs/MWCNTs/SPE electrode. This modification was performed with CV by applying potential ranging from −0.2 to +0.6 V for 15 cycles (scan rate of 20 mV/s). To remove the template from MIP, the electrode surface was further washed 3 times each for 15 min using a mixture of methanol and acetic acid and kept for drying at room temperature. The fabrication steps involved in the development of an electrode are step-wise illustrated in Scheme 2.

2.5.5. Evaluation of the fabricated Co_3O_4NPs/MnO_2NSs/MWCNTs/SPE electrode

The fabricated surface of the electrode after every modification was studied with SEM imaging. The reaction response on the electrode surface was determined with electrochemical measurements (cyclic voltammetry, differential pulse voltammetry (DPV), and electrochemical impedance spectroscopy (EIS)).

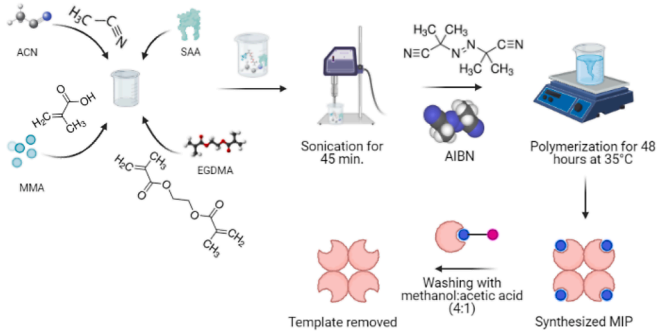

ACN: Acetonitrile (Porogen); SAA: Serum Amyloid A (Template); EGDMA: Ethylene glycol dimethacrylate (Crosslinker); MMA: Methyl methacrylate (Monomer); AIBN: Azobisisobutyronitrile (Initiator); MIP: Molecularly imprinted polymer

Scheme 1. Graphical representation of the steps involved in molecularly imprinted polymer (MIP) synthesis with serum amyloid A (SAA) as a template.

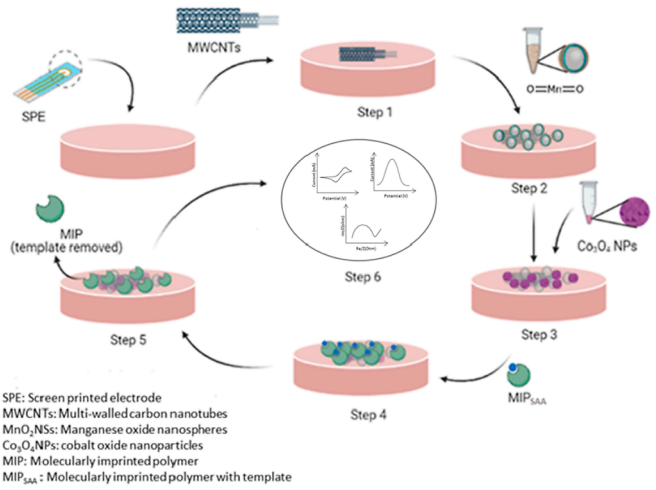

Scheme 2. Schematic illustration of the developed biosensor
Step 1: Electrodeposition of multi-walled carbon nanotubes (MWCNTs) on the bare screen-printed electrode (SPE).
Step 2: Modification of MWCNTs/SPE with manganese dioxide nanospheres (MnO_2NSs).
Step 3: Electrodeposition of cobalt oxide nanoparticles (Co_3O_4NPs) on modified MnO_2NSs/MWCNTs/SPE electrode.
Step 4: Deposition of molecularly imprinted polymer (MIP_{SAA}) on Co_3O_4NPs/MnO_2NSs/MWCNTs/SPE electrode.
Step 5: Removal of template from the imprinted polymer.
Step 6: Electrochemical measurements for the fabricated biosensor.

The electrode was optimized with varying pH within a range from 5.5 to 8.5 and temperature from 10 °C to 80 °C. Further, the stability of the system was observed at different scan rates from 20 to 140 mV/s. Moreover, the electrode response was observed with various interfering factors including ascorbic acid, cholesterol, glucose, uric acid, acetylcholine.

2.5.6. Examination of the developed biosensor with clinical samples

Finally, the electrode was examined with clinical samples of neonates obtained from the Bio Diagnostics Lab, New Delhi, India. The serum samples were pre-treated for lipoprotein extraction and afterward, the experiments were performed.

3. Results and discussion

3.1. Surface modification of the fabricated MIP/Co_3O_4NPs/MnO_2NSs/MWCNTs/SPE electrode

The surface of the developed sensor was characterized with SEM at every modification step, as shown in Fig. 1. The rough tube structures were obtained by MWCNTs modification as visible in Fig. 1(a). The MWCNTs provide large surface area, high electrical conductivity, and great support for biomolecules [35]. Fig. 1(b) shows the surface of the electrode after MnO_2NSs deposition. The unique properties of MWCNTs provide immense support to MnO_2NSs for utilizing the optimal active sites on the electrode. Besides, the MnO_2NSs possess high energy density, catalytic ability and are low-cost. Fig. 1(c) depicts the spherical structure of Co_3O_4NPs on the surface of assembled MnO_2NSs/MWCNTs/SPE electrode. Further, the MIP prepared for SAA was electrodeposited on the electrode surface as shown in Fig. 1(d). The micrographs show a similar imprint of the template molecule over the surface of the electrode. The prepared MIP was washed to remove SAA molecules from the imprinted structures. After the removal of a template, the cavities were obtained on the surface of the working electrode as illustrated in Fig. 1 (e). For control experiments, non-imprinted polymer (NIP) was synthesized. The synthesis of NIP was carried out with monomer,

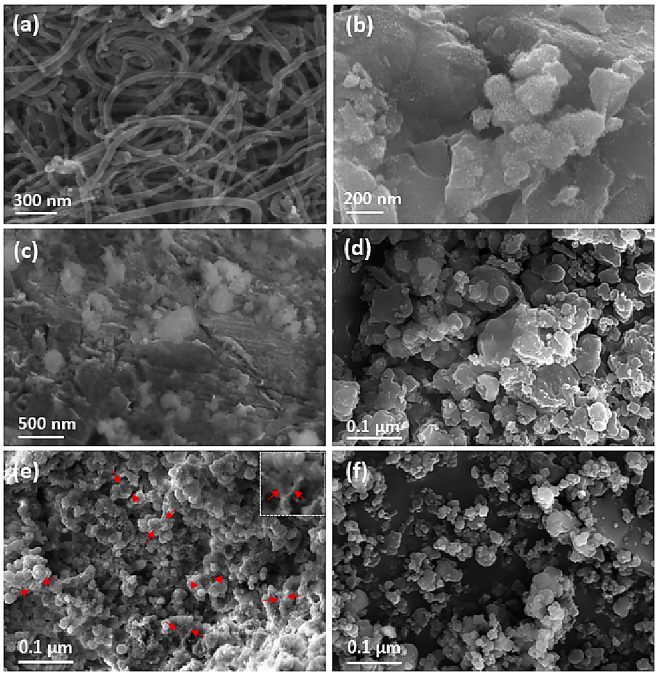

Fig. 1. Scanning electron microscopy (a) MWCNTs/SPE, (b) MnO_2NSs /MWCNTs/SPE, (c) Co_3O_4NPs/MnO_2NSs/MWCNTs/SPE, (d) MIP_{SAA}/ Co_3O_4NPs/MnO_2NSs/MWCNTs/SPE, and (e) MIP/Co_3O_4NPs/MnO_2NSs/ MWCNTs/SPE (arrow: shows the imprints (cavities) of SAA molecule), (f) Non-imprinted polymer (NIP)/Co_3O_4NPs/MnO_2NSs/MWCNTs/SPE.

crosslinker, and porogen in the absence of a template. Fig. 1(f) illustrates the SEM micrographs for NIP.

Fig. 2 describes the XRD pattern for MIP, NIP, and MIP_{SAA}. The diffraction peaks were obtained at 17.74, 17.86, 17.26 for MIP, NIP, and MIP_{SAA} respectively. The shifting of the diffraction peak towards a lesser 2θ value implies an increment in the interlayer spacing [36]. While the decreasing intensity of the diffraction peak describes monomer and template interaction [36].

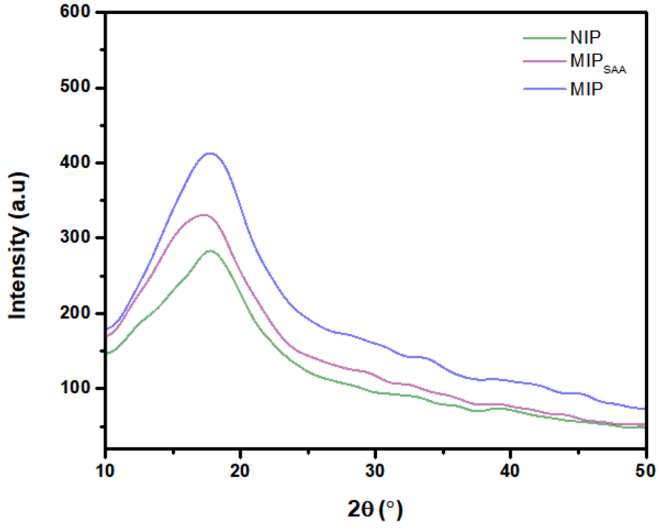

Fig. 2. X-Ray Diffraction (XRD) analysis for synthesized (i) NIP, (ii) MIP_{SAA}, and (iii) MIP.

3.2. Electrochemical studies for the developed biosensor

3.2.1. Stepwise modification of the fabricated MIP/Co_3O_4NPs/MnO_2NSs/MWCNTs/SPE electrode

The response of the electrode for each modification stage was recorded by CV. Fig. 3(a) shows CV curves obtained in Ferri-Ferro mediator (0.5 mM) solution when applying a potential from −1.0 to +1.0 V. The minimum oxidation and reduction peaks were obtained with the bare electrode in the mediator solution. Firstly, the electrode surface was modified with MWCNTs to magnify the electrochemical activity of the sensor. The oxidation and reduction peak current, in this case, was increased up to +3.15 mA and − 2.98 mA respectively. Secondly, the surface of the MWCNTs/SPE electrode was moderated with MnO_2NSs to improve the catalytic activity of the biosensor. It was observed that the oxidation (+3.7 mA) and reduction (−3.5 mA) peaks current was enhanced. Furthermore, at the third step, the electrode was altered with Co_3O_4NPs. The observed response of the electrode describes that the maximum oxidation and reduction peaks were obtained with Co_3O_4NPs. This is due to the synergistic effect of Co_3O_4NPs/MnO_2NSs/ MWCNTs. Further, the MIP_{SAA} was electrodeposited on the surface of the working electrode, and the CV response was obtained. The oxidation and reduction peaks decrease after the MIP deposition. The presence of polymer on the electrode surface restricts the flow of current therefore a decline in the oxidation and reduction peaks were observed. The deposited MIP on the electrode surface was washed 3 times. The CV curve obtained after template removal shows enhancement in oxidation and reduction peaks.

The response of the electrode was further recorded with EIS as shown in Fig. 3(b). The Nyquist plot in the graph describes the diffusion process (linear part) and resistance charge transfer (Rct) (semi-circle) on the modified electrode surface. The EIS graph illustrates that the higher Rct value was obtained for the bare electrode, and it gradually decreases once the electrode was modified with MWCNTs, MnO_2NSs, and Co_3O_4NPs, respectively. Further, the modification of electrode surface with MIP_{SAA} provides an increased Rct value by generating a higher resistance. The template was then washed out from the molecularly imprinted polymer surface causing the Rct value to decrease on the electrode.

3.2.2. Concentration study for SAA on MIP/Co_3O_4NPs/MnO_2NSs/MWCNTs/SPE electrode

The electrode was evaluated with varying concentrations of SAA. The response for different concentrations was obtained with electrochemical impedance spectroscopy and differential potential voltammetry as presented in Fig. 4(a) and (b), respectively. The electrode was evaluated within a concentration range from 0.01 pM to 1 μM (0.01 pM, 0.1 pM, 1 pM, 10 pM, 0.1 nM, 1 nM, 10 nM, 0.1 μM, 1 μM). The Nyquist plot in Fig. 4(a) describes the Rct value for varying concentrations. It was observed that with increasing concentration from 0.01 pM to 1 μM, the Rct value gradually increases.

The current response of the electrode at varying concentrations was recorded with DPV as shown in Fig. 4(b). The obtained results describe that the current peak decreases with increasing concentrations. At higher concentrations, the active sites on the electrode surface are blocked causing a low current generation and higher resistance.

3.3. Optimizing parameters for working MIP/Co_3O_4NPs/MnO_2NSs/MWCNTs/SPE electrode

3.3.1. Evaluating the electrode on various pH values

To obtain the optimum pH for the working electrode, it was examined within a range of pH solutions from pH 5.5 to 8.5, with an interval of 0.5 pH units (Fig. 5(a)). The pH studies were performed in an electron mediator (0.5 mM) with an optimized 0.01 pM concentration of SAA. Fig. 5(b) depicts the bar graph for peak current values obtained from DPV curves. The graph represents an increase in the peak current from

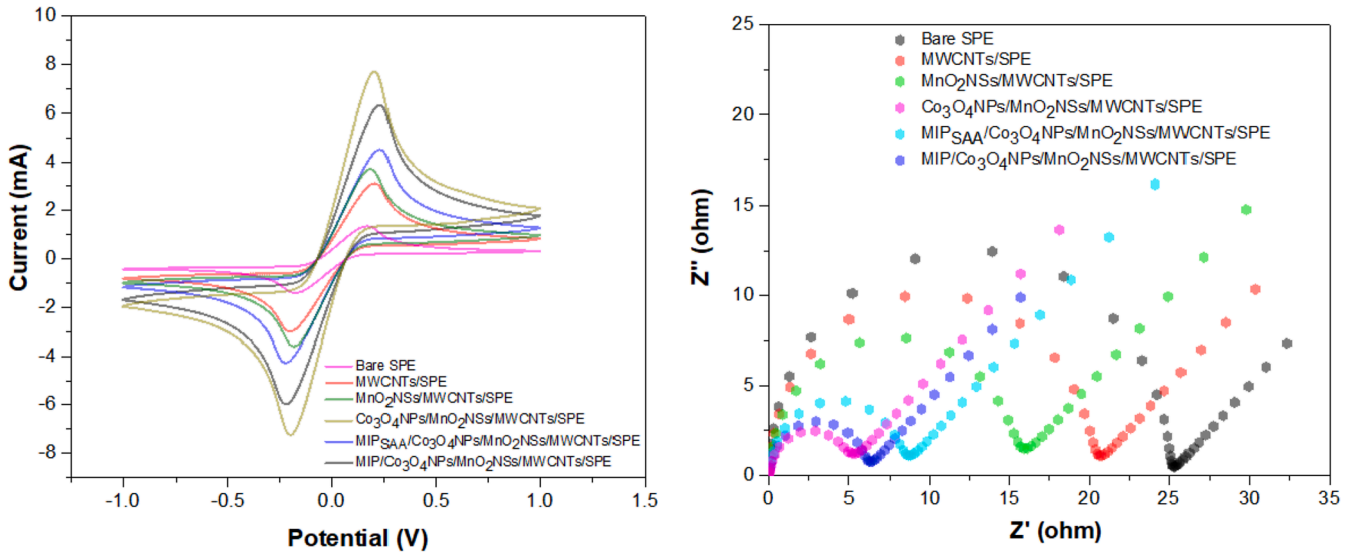

Fig. 3. Electrode modification: (a) Cyclic voltammetry (CV) was carried out in a Ferri-Ferro mediator solution of 0.5 mM for bare SPE, MWCNTs/SPE, MnO_2NSs/MWCNTs/SPE, Co_3O_4NPs/MnO_2NSs/MWCNTs/SPE, MIP_{SAA}/Co_3O_4NPs/MnO_2NSs/MWCNTs/SPE, and MIP/Co_3O_4NPs/MnO_2NSs/MWCNTs/SPE, within a potential range from −1.0 to +1.0 V (scan rate 50 mV/s).
(b) Electrochemical impedance spectroscopy (EIS) studies were carried out in a mediator solution at frequencies: $F_{initial}$-100 khz and F_{final}-100 mhz for bare SPE, MWCNTs/SPE, MnO_2NSs/MWCNTs/SPE, Co_3O_4NPs/MnO_2NSs/MWCNTs/SPE, MIP_{SAA}/Co_3O_4NPs/MnO_2NSs/MWCNTs/SPE, and MIP/Co_3O_4NPs/MnO_2NSs/MWCNTs/SPE.

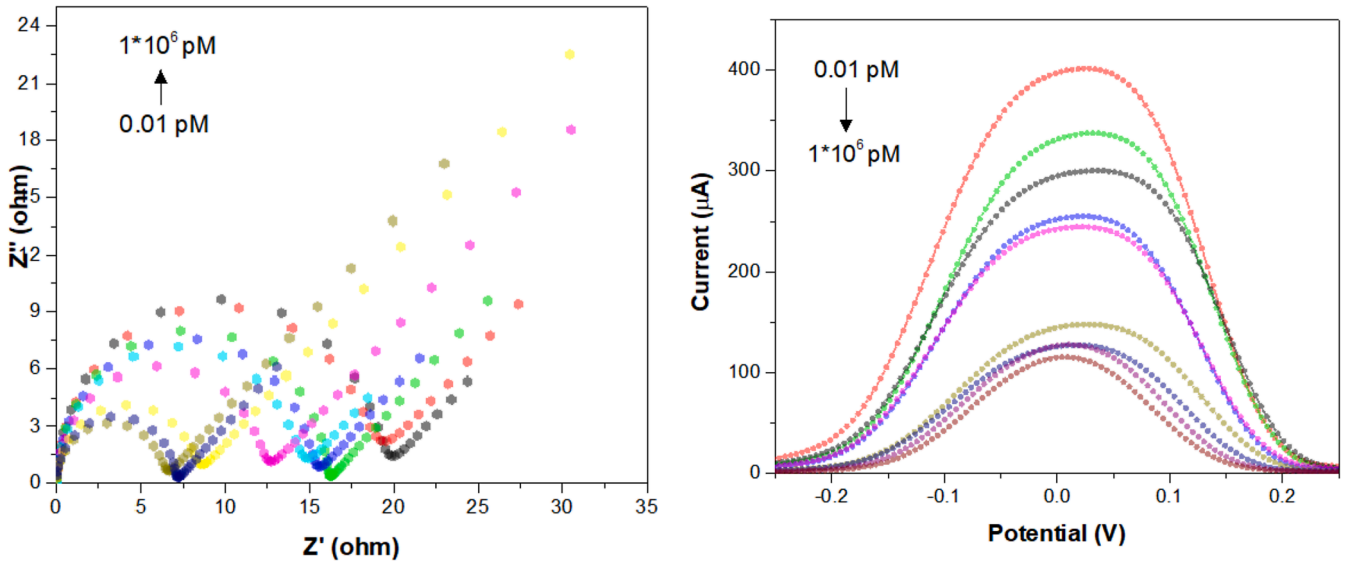

Fig. 4. Concentration studies: (a) Impedance and (b) Differential pulse voltammetry (DPV) studies for serum amyloid A (SAA) concentration (0.01 pM, 0.1 pM, 1 pM, 10 pM, 0.1 nM, 1 nM, 10 nM, 0.1 μM, 1 μM) on developed MIP/Co_3O_4NPs/MnO_2NSs/MWCNTs/SPE electrode at frequencies: $F_{initial}$-100 Khz and F_{final}-100 mhz in a mediator solution of Ferri-Ferro (0.5 mM).

pH 5.5 to 6 and after pH 6, the peak current decreases continuously. The hydrogen bonds formed between the template and polymer cause an enhancement in resistance on the electrode surface and thereby decrease the charge flow [37].

3.3.2. Scan rate study for the working electrode

The scan rate study was determined to understand steady electron-transfer kinetics on the surface of the assembled electrode. The scan rate study was carried out in an electron mediator solution (0.5 mM), applying a constant potential from −0.5 to +1.0 V. Fig. 5(c) describes the CV curve for varying scan rates ranging from 20 to 140 mV/s with an interval of 20 mV/s. Once the scan rate is increased from 20 to 140 mV/s, the anodic and cathodic peaks are enhanced at a constant potential. As shown in Fig. 5(d), a calibration curve was plotted for the anodic and cathodic peak versus the square root value of scan rates.

3.3.3. Interference studies on the working electrode

The working electrode was studied with different interfering compounds such as ascorbic acid ($C_6H_8O_6$) (0.05 mM), cholesterol ($C_{27}H_{46}O$) (2.00 g/L), glucose ($C_6H_{12}O_6$) (5 mM), uric acid ($C_5H_4N_4O_3$) (0.2 mM), and acetylcholine (Ach) (0.1 mM) in their physiological range [38,39]. The interference study was performed in a mediator solution (0.5 mM) at potential +0.2 V, containing a 0.01 pM concentration of SAA. The loss of biosensor activity (%) for various interfering compounds is presented in Fig. 5(e). The percentage loss of activity of the biosensor was calculated and the maximum loss of activity was obtained

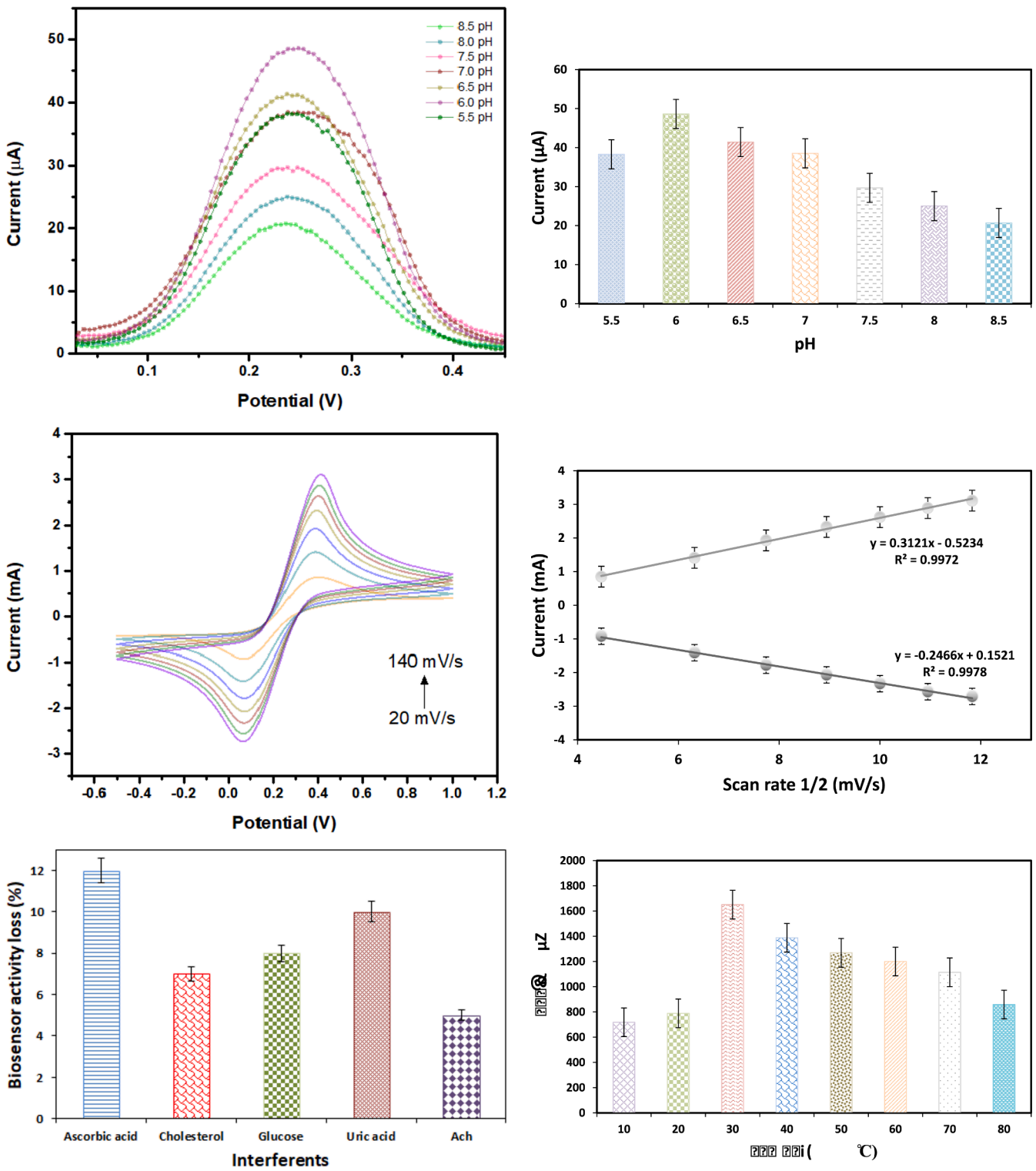

Fig. 5. Optimization of the developed biosensor

(a) Differential pulse voltammetry studies for the effect of pH values (5.5, 6.0, 6.5, 7.0, 7.5, 8.0, 8.5) on the developed MIP/Co_3O_4NPs/MnO_2NSs/MWCNTs/SPE electrode.

(b) The bar graph represents a plot for peak current vs pH value.

(c) Evaluation of developed biosensor at variable scan rate from 20 to 140 mV/s at an interval of 20, in a Ferri-Ferro mediator solution of 0.5 mM and within a constant potential range from −0.5 to +1.0 V.

(d) The linear graph describes the relation for a peak current of the CV curve for scan rate and the square root of scan rate.

(e) Interference study on the fabricated biosensor with different interferents like ascorbic acid, cholesterol, glucose, uric acid, acetylcholine (Ach) with an optimized SAA concentration (0.01 pM) in a 0.5 mM electron mediator solution.

(f) Analysis of varying temperature for the developed sensor within a range from 10 to 80° C with an interval of 10° C at −0.5 V.

(g) Reproducibility of the data for the developed biosensor with 20 identically prepared electrodes and maintaining the same conditions.

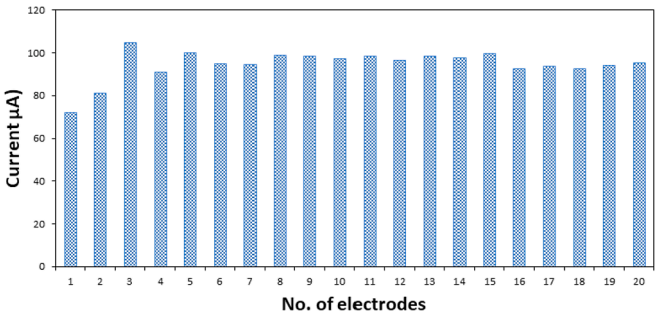

Fig. 5. (*continued*).

with ascorbic acid (12%) and the minimum was recorded with Ach (5%). Whereas, cholesterol (7%), glucose (8%), and uric acid (10%) show their loss of activity in the range of 5% to 12%.

3.3.4. Optimization of temperature for modified electrode

The fabricated biosensor was evaluated with varying temperatures, within a range from 10° C to 80° C, at an interval of 10° C. The study was performed in an electron mediator (0.5 mM) with 0.01 pM SAA concentration. A bar graph was plotted for temperature versus current as presented in Fig. 5(f). The peak current increases from 10° C to 30° C and continuously decreases beyond 30° C. Therefore, 30° C was selected as an optimum temperature for the working electrode.

3.4. Reproducibility and stability of the working electrode

The reproducibility of the obtained data was confirmed by 20 identical electrodes prepared under similar conditions. Fig. 5(g) describes the current obtained from 20 similarly prepared electrodes, the relative standard deviation (RSD) value calculated for the developed electrodes was 7.55%.

The stability of the developed biosensor was evaluated for 3 months while the electrode response was checked every seventh day. The electrode was stored at 4° C in dry condition. After 6 weeks, the activity of the electrode was reduced to 50%. The results for the developed biosensor are summarized in Table 1. The developed biosensor was compared with reported studies as represented in Table 2. It was observed that the fabricated sensing platform exhibits a lower detection limit and wide concentration range than the reported sensors.

3.5. Validation of developed biosensor with clinical samples

The developed MIP/Co_3O_4NPs/MnO_2NSs/MWCNTs/SPE electrode was validated with serum samples. The serum samples of neonates were acquired from Bio Diagnostics Lab, New Delhi, India. To separate lipoprotein from serum, the samples were pre-treated with salt solutions (sodium chloride and potassium bromide). Further, for 1 mL of serum sample, ultracentrifugation was carried out at 12 to 15° C. Thereafter, a thin film of lipoprotein was formed on the top and beneath a clear solution was obtained [44,45]. Further, the results of the developed biosensor were compared with the standard ELISA method. Fig. 6 shows a correlation graph for the result obtained with the present work and ELISA method for SAA detection (regression coefficient = 0.988).

Table 1
Summary of the parameters obtained for developed electrochemical biosensor for SAA detection.

S.No.	Parameter	Value
1.	Detection limit	0.01 pM
2.	Linear range	0.01 pM - 1 µM
3.	Sample volume	<10 µL
4.	Response time	< 3 min
5.	Sensitivity	0.47 µA/pM

Table 2
Comparison of parameters for developed MIP/Co_3O_4NPs/MnO_2NSs/MWCNTs/SPE electrode with reported studies.

S. No.	Sensing platform	Limit of detection	Detection range	References
1.	Fe_3O_4@Au SERS tags-based LFA	0.1 ng/mL	0.1–500 ng/mL	[40]
2.	Sandwich-type, antibody microarrays	5.9 ng/mL	5.9–478 ng/mL	[41]
3.	MWCNTs/IL/Chit/GC electrode	0.3 pg/mL	0.001–900 ng/mL	[42]
4.	Quantum dots-based fluorescence-linked immunosorbent assay	2.39 ng/mL	10–1000 ng/mL	[43]
5.	MIP/Co_3O_4NPs/MnO_2NSs/MWCNTs/SPE	0.12 pg/mL	0.12 pg/mL-12 µg/mL	Present work

Ferric oxide (Fe_3O_4); Gold (Au); Surface-enhanced Raman scattering (SERS); Lateral flow assay (LFA); Multi-walled carbon nanotubes (MWCNTs); Ionic liquid (IL); Chitosan (Chit); Glassy carbon (GC); Molecularly imprinted polymer (MIP); Cobalt oxide nanoparticles (Co_3O_4NPs); Manganese oxide nanospheres (MnO_2NSs); Screen-printed electrode (SPE).

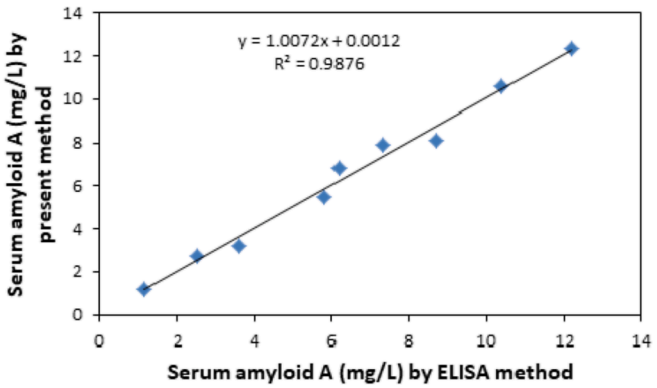

Fig. 6. Correlation graph for values obtained with developed method versus standard ELISA method for SAA detection.

4. Conclusion

A biosensor for the detection of serum amyloid A was developed which was based upon the molecularly imprinted polymer technique by modifying the electrode surface for detecting SAA concentration. The electrode was modified with nanomaterials for amplifying electrochemical properties. To increase the surface area of the fabricated electrode, it was modified with MWCNTs. The catalytic performance and conductivity of the electrode were further triggered by MnO_2NSs and Co_3O_4NPs. The MIP/Co_3O_4NPs/MnO_2NSs/MWCNTs/SPE electrode

was then examined with varying concentrations of SAA. This developed biosensor operates in a wide concentration range from 0.01 pM to 1 μM and indicates a lower limit of detection as 0.01 pM. The half-life of the MIP/Co_3O_4NPs/MnO_2NSs/MWCNTs/SPE electrode was 42 days. The modification of the electrode with nanoparticles and molecularly imprinted polymer facilitates improving analytical properties of the sensing platform such as higher sensitivity, specificity, and reproducibility. This fabricated biosensor can be developed into a portable and point of care (POC) device for fast and early detection of neonatal sepsis.

Declaration of competing interest

The authors here declare no personal or financial conflict of interest for the presented work.

Acknowledgments

The work is financially supported by the Extramural Research grant (File No. EMR/2016/007564) and Young Scientist Scheme (File No. YSS/2015/000023) of the Science and Engineering Research Board, Government of India, and Technology Development Program (TDP) (TDP/BDTD/33/2019) of Department of Science and Technology (DST), Government of India and by Department of Biotechnology (DBT) (BT/PR36874/MED/97/475/2020), Government of India.

Data availability

The raw/processed data required to reproduce these findings cannot be shared at this time as the data also forms part of an ongoing study.

References

[1] H. Yuan, J. Huang, B. Lv, W. Yan, G. Hu, J. Wang, B. Shen, Diagnosis value of the serum amyloid A test in neonatal sepsis: a meta-analysis, Biomed. Res. Int. 2013 (2013).
[2] G.M. Elmashad, H.M. Elsayed, Z.A. Omar, E.A. Badr, O.M. Omran, Evaluation of serum amyloid A protein as a marker in neonatal sepsis, Menoufia Med. J. 32 (2019) 1094.
[3] B.V. Bhat, P. Prasad, V.B.R. Kumar, B.N. Harish, K. Krishnakumari, A. Rekha, G. Manjunath, B. Adhisivam, B. Shruthi, Syndrome evaluation system (SES) versus blood culture (BACTEC) in the diagnosis and management of neonatal sepsis-a randomized controlled trial, Indian Journal of Pediatrics 83 (2016) 370–379.
[4] N. Chauhan, S. Tiwari, U. Jain, Potential biomarkers for effective screening of neonatal sepsis infections: an overview, Microb. Pathog. 107 (2017) 234–242.
[5] S. Balayan, N. Chauhan, R. Chandra, N.K. Kuchhal, U. Jain, Recent advances in developing biosensing based platforms for neonatal sepsis, Biosens. Bioelectron. 25 (2020), 112552.
[6] A.L. Ramby, D.M. Goodman, E.L. Wald, S.L. Weiss, Red blood cell distribution width as a pragmatic marker for outcome in pediatric critical illness, PloS one 10 (2015), e0129258.
[7] M. Cetinkaya, H. Özkan, N. Köksal, S. Celebi, M. Hacımustafaoğlu, Comparison of serum amyloid A concentrations with those of C-reactive protein and procalcitonin in diagnosis and follow-up of neonatal sepsis in premature infants, Journal of Perinatology 29 (2009) 225–231.
[8] S. Arnon, I. Litmanovitz, R.H. Regev, S. Bauer, R. Shainkin-Kestenbaum, T. Dolfin, Serum amyloid A: an early and accurate marker of neonatal early-onset sepsis, Journal of Perinatology 27 (2007) 297–302.
[9] M.Y. Memar, N. Alizadeh, M. Varshochi, H.S. Kafil, Immunologic biomarkers for diagnostic of early-onset neonatal sepsis, The Journal of Maternal-Fetal & Neonatal Medicine 32 (2019) 143–153.
[10] D. Sharma, N. Farahbakhsh, S. Shastri, P. Sharma, Biomarkers for diagnosis of neonatal sepsis: a literature review, The Journal of Maternal-Fetal & Neonatal Medicine 31 (2018) 1646–1659.
[11] M.F. Osuchowski, D.G. Remick, The repetitive use of samples to measure multiple cytokines: the sequential ELISA, Methods 38 (2006) 304–311.
[12] E.A. Morad, R.A. Rabie, M.A. Almalky, M.G. Gebriel, Evaluation of procalcitonin, C-reactive protein, and interleukin-6 as early markers for diagnosis of neonatal sepsis, International journal of microbiology 2020 (2020), 8889086.
[13] S. Sakamoto, W. Putalun, S. Vimolmangkang, W. Phoolcharoen, Y. Shoyama, H. Tanaka, S. Morimoto, Enzyme-linked immunosorbent assay for the quantitative/qualitative analysis of plant secondary metabolites, Journal of natural medicines 72 (2018) 32–42.
[14] S.B. Nimse, M.B. Sonawane, K.S. Song, T. Kim, Biomarker detection technologies and future directions, Analyst 141 (2016) 740–755.
[15] N. Chauhan, S. Balayan, U. Jain, Sensitive biosensing of neurotransmitter: 2D material wrapped nanotubes and MnO2 composites for the detection of acetylcholine, Synth. Met. 263 (2020), 116354.
[16] J. Chen, W.D. Zhang, J.S. Ye, Nonenzymatic electrochemical glucose sensor based on MnO2/MWNTs nanocomposite, Electrochem. Commun. 10 (2008) 1268–1271.
[17] M. Wang, C. Wang, G. Wang, W. Zhang, F. Bin, Synthesis of MnO2/MWNTs nanocomposites using a sonochemical method and application for hydrazine detection, electroanalysis: an international journal devoted to fundamental and practical aspects ofElectroanalysis 22 (2010) 1123–1129.
[18] A.B. Zakaria, R. Nuringtyas, A. Hardoyo, Special protection system with macro VBA-based descending method at PT PLN (Persero) South and Central Kalimantan, in: 2019 International Conference on Technologies and Policies in Electric Power & Energy IEEE, 2019, pp. 1–4.
[19] F. Lyu, Y. Bai, Q. Wang, L. Wang, X. Zhang, Y. Yin, Coordination-assisted synthesis of iron-incorporated cobalt oxide nanoplates for enhanced oxygen evolution, Mater. Today Chem. 11 (2019) 112–118.
[20] S. Nallusamy, K. Sujatha, Experimental analysis of nanoparticles with cobalt oxide synthesized by coprecipitation method on electrochemical biosensor using FTIR and TEM, Mater. Today Proc. 37 (2021) 728–732.
[21] S. Nallusamy, Thermal conductivity analysis and characterization of copper oxide nanofluids through different techniques, Journal of Nano Research 40 (2016) 105–112.
[22] O.I. Medvedeva, S.S. Kambulova, O.V. Bondar, A.R. Gataulina, N.A. Ulakhovich, A. V. Gerasimov, V.G. Evtugyn, I.F. Gilmutdinov, M.P. Kutyreva, Magnetic cobalt and cobalt oxide nanoparticles in hyperbranched polyester polyol matrix, J. Nanotechnol. 2017 (2017), 7607658.
[23] M. Rashad, M. Rüsing, G. Berth, K. Lischka, A. Pawlis, CuO and Co3O4 nanoparticles: synthesis, characterizations, and Raman spectroscopy, J. Nanomater. 2013 (2013), 714853.
[24] L. Uzun, A.P. Turner, Molecularly-imprinted polymer sensors: realising their potential, Biosens. Bioelectron. 76 (2016) 131–144.
[25] B.B. Yücebaş, Y.T. Yaman, G. Bolat, E. Özgür, L. Uzun, S. Abaci, Molecular imprinted polymer based electrochemical sensor for selective detection of paraben, Sensors Actuators B Chem. 305 (2020), 127368.
[26] C. Yang, X.F. Ji, W.Q. Cao, J. Wang, Q. Zhang, T.L. Zhong, Y. Wang, Molecularly imprinted polymer based sensor directly responsive to attomole bovine serum albumin, Talanta 196 (2019) 402–407.
[27] U. Jain, S. Soni, Y.P.S. Balhara, M. Khanuja, N. Chauhan, Dual-layered nanomaterial-based molecular pattering on polymer surface biomimetic impedimetric sensing of a bliss molecule,anandamide neurotransmitter, ACSOmega 5 (2020) 10750–10758.
[28] H.H. Wang, X.J. Chen, W.T. Li, W.H. Zhou, X.C. Guo, W.Y. Kang, D.X. Kou, Z. J. Zhou, Y.N. Meng, Q.W. Tian, S.X. Wu, ZnO nanotubes supported molecularly imprinted polymers arrays as sensing materials for electrochemical detection of dopamine, Talanta 176 (2018) 573–581.
[29] A.A. Lahcen, F. Arduini, F. Lista, A. Amine, Label-free electrochemical sensor based on spore-imprinted polymer for Bacillus cereus spore detection, Sensors Actuators B Chem. 276 (2018) 114–120.
[30] Y. Li, W. Xu, X. Zhao, Y. Huang, J. Kang, Q. Qi, C. Zhong, Electrochemical sensors based on molecularly imprinted polymers on Fe3O4/graphene modified by gold nanoparticles for highly selective and sensitive detection of trace ractopamine in water, Analyst 143 (2018) 5094–5102.
[31] F. Lopes, J.G. Pacheco, P. Rebelo, C. Delerue-Matos, Molecularly imprinted electrochemical sensor prepared on a screen printed carbon electrode for naloxone detection, Sensors Actuators B Chem. 243 (2017) 745–752.
[32] X. Fu, J. Feng, H. Wang, K.M. Ng, Fast synthesis and formation mechanism of γ-MnO2 hollow nanospheres for aerobic oxidation of alcohols, Mater. Res. Bull. 45 (2010) 1218–1223.
[33] Y. Dong, K. He, L. Yin, A. Zhang, A facile route to controlled synthesis of Co3O4 nanoparticles and their environmental catalytic properties, Nanotechnology 18 (2007), 435602.
[34] R. Rawal, S. Chawla, N. Chauhan, T. Dahiya, C.S. Pundir, Construction of amperometric uric acid biosensor based on uricase immobilized on PBNPs/cMWCNT/PANI/Au composite, Int. J. Biol. Macromol. 50 (2012) 112–118.
[35] J. Narang, U. Jain, N. Malhotra, S. Singh, N. Chauhan, Development of lysine biosensor based on core shell magnetic nanoparticle and multiwalled carbon nanotube composite, Adv. Mater. Lett. 6 (2015) 407–413.
[36] T. Nurhayati, I. Royani, Synthesis and characterization of MAA-based molecularly-imprinted polymer (MIP) with D-glucose template, in: Journal of Physics: Conference Series, 739, IOP Publishing, 2016, p. 012143.
[37] N.A. Yusof, S.K.A. Rahman, M.Z. Hussein, N.A. Ibrahim, Preparation and characterization of molecularly imprinted polymer as SPE sorbent for melamine isolation, Polymers 5 (2013) 1215–1228.
[38] R. Rawal, S. Chawla, N. Chauhan, T. Dahiya, C.S. Pundir, Construction of amperometric uric acid biosensor based on uricase immobilized on PBNPs/cMWCNT/PANI/Au composite, Int. J. Biol. Macromolecules (2012) 112–118.
[39] C.S. Pundir, J. Narang, N. Chauhan, P. Sharma, R. Sharma, An amperometric cholesterol biosensor based on epoxy resin membrane bound cholesterol oxidase, Indian J. Med. Research (2012) 633–640.
[40] X. Liu, X. Yang, K. Li, H. Liu, R. Xiao, W. Wang, C. Wang, S. Wang, Fe3O4@ Au SERS tags-based lateral flow assay for simultaneous detection of serum amyloid A and C-reactive protein in unprocessed blood sample, Sensors and Actuators B: Chemical 320 (2020), 128350.
[41] O. Gul, E. Calay, U. Sezerman, H. Basaga, Y. Gurbuz, Sandwich-type, antibody microarrays for the detection and quantification of cardiovascular risk markers, Sensors Actuators B Chem. (2007) 581–588.

[42] C. Xia, Y. Li, G. Yuan, Y. Guo, C. Yu, Immunoassay for serum amyloid A using a glassy carbon electrode modified with carboxy-polypyrrole, multiwalled carbon nanotubes, ionic liquid and chitosan, Microchim. Acta (2015) 1395–1402.
[43] Y. Lv, F. Wang, N. Li, R. Wu, J. Li, H. Shen, L.S. Li, F. Guo, Development of dual quantum dots-based fluorescence-linked immunosorbent assay for simultaneous detection on inflammation biomarkers, Sensors and Actuators B: Chemical 301 (2019), 127118.
[44] G.R. Warnick, M. Nauck, N. Rifai, Evolution of methods for measurement of HDL-cholesterol: from ultracentrifugation to homogeneous assays, Clin. Chem. (2001) 1579–1596.
[45] R.J. Havel, H.A. Eder, J.H. Bragdon, The distribution and chemical composition of ultracentrifugally separated lipoproteins in human serum, J. Clin. Invest. (1955) 1345–1353.